2017 Accomplishments – Tritium Aging Studies on Stainless Steel Weldments and Heat-Affected Zones

MICHAEL J. MORGAN, DALE HITCHCOCK, TIM KRENTZ, JOY MCNAMARA, AND ANDREW DUNCAN

Materials Science and Technology

Publication Date: January 2018

Savannah River National Laboratory
Savannah River Nuclear Solutions, LLC
Aiken, SC 29808

DISCLAIMER

2017 Accomplishments – Tritium Aging Studies on Stainless Steel Weldments and Heat-Affected Zones

CONTENTS   **PAGE**

List of Figures   **Page**

List of Tables   **Page**

TRITIUM AGING STUDIES ON STAINLESS STEEL WELDMENTS AND HEAT-AFFECTED ZONES

I. SUMMARY

In support of Enhanced Surveillance, "Tritium Effects on Materials", the fracture toughness properties of long-aged tritium-charged stainless-steel base metals and weldments were measured and compared to earlier measurements. The fracture-toughness data were measured by thermally precharging as-forged and as-welded specimens with tritium gas at 34.5 MPa and 350°C and aging for approximately 17 years to build-in decay helium prior to testing. These data result from the longest aged specimens ever tested in the history of the tritium effects programs at Savannah River and the fracture toughness values measured were the lowest ever recorded for tritium-exposed stainless steel. For Type 21-6-9 stainless steel, fracture toughness values were reduced to less than 2-4% of the as-forged values to 41 lbs / in specimens that contained more than 1300 appm helium from tritium decay. The fracture toughness properties of long-aged weldments were also measured. The fracture toughness reductions were not as severe because the specimens did not retain as much tritium from the charging and aging as did the base metals. For Type 304L weldments, the specimens in this study contained approximately 600 appm helium and their fracture toughness values averaged 750 lbs / in. The results for other steels and weldments are reported and additional tests will be conducted during FY18.

The trend of decreasing fracture toughness values with increased helium content is consistent with earlier observations on Type 21-6-9 stainless steel, and the data continue to show that Type 304L stainless steel is more resistant to tritium-induced cracking than Type 21-6-9 stainless at similar decay helium levels. While the data show that fracture toughness values of the weldments of both steels are similar at all helium levels, decay helium measurements confirm the difficulty with conducting tritium effects testing on weldments in air environments. The weldments retain much less tritium than austenitic stainless steels base metals because of enhanced off-gassing losses during cool down from charging temperatures and aging at low temperatures due to the presence of ferrite in the weld which lowers hydrogen solubility and provides a high-hydrogen diffusion path out of the material.

In addition to the tritium-effects fracture testing, significant progress on new activities are reported. First, fracture toughness specimens fabricated from Types 304L and 21-6-9 stainless steel weldments and heat-affected zones (HAZ) were exposed to tritium gas. The specimens were prepared by Sandia National Laboratory and the data will be "first of kind" in that the fracture toughness properties of tritium-exposed heat affected zones has never been measured. Secondly, Small-Angle-Neutron Scattering(SANS) measurements were conducted on tritium-exposed stainless steels including some of the long-aged specimens described above. SANS is being explored as a technique to quantify decay helium bubble gas densities, size, spacing, and distribution in alloys. The data are needed to develop fracture models on the effects of hydrogen isotopes and helium on stainless steel and will complement transmission electron microscopy (TEM) characterizations. TEM facilities are being

upgraded and new researchers trained for developing techniques for decay-helium bubble microstructure characterizations in the long-aged specimens and the new weld heat-affected zone specimens. Joint efforts with Sandia are planned. Finally, a new imaging technique, Kelvin-Probe-Force microscopy, is being used to gain a better understanding of hydrogen trapping effects in steel. The technique is able to provide images of hydrogen co-located in the interfaces like grain and twin boundaries in steel microstructures.

II. INTRODUCTION

The effects of tritium on the fracture properties of stainless steels and its weldments vary with the steel type and microstructure (1-12). Typical tritium reservoirs have three main microstructural regions: Forged base material; Weldment; and Weld HAZ. Because of tritium aging effects, fracture mechanics properties and steel behavior as a function of tritium and decay helium content in a variety of steel microstructures are needed for fracture modeling, reservoir life prediction, and safety margin evaluations (5– 8).

In this study, the combined effects tritium and decay helium in forged and welded Types 304L and 21-6-9 stainless steels were studied. To measure these effects, fracture mechanic specimens were thermally precharged with tritium and aged for approximately 17 years to build in decay helium from tritium decay prior to testing. The results are compared to earlier measurements on the same alloys and weldments (4-5, 8-9).

Also progress on three new programs were initiated for characterizing tritium and decay helium on containment alloys and are reported. Weldments and HAZ specimens were tritium pre-charged and will be tested after aging times of up to five years. Initial tests on three-month aged specimens will be conducted in 2Q18. Transmission-electron microscopy facilities are being upgraded for characterizations of material and decay helium bubble microstructures on long-aged specimen, HAZ specimens, and additive manufactured alloys. Finally, a new technique for imaging hydrogen in materials, Kelvin Probe Force microscopy, is being investigated for its potential to reveal hydrogen co-located on microstructural features.

III. EXPERIMENTAL PROCEDURE

For this continuing study, forged and welded steels of prior studies were used. The composition of the steels and weld filler materials are the same as those used before (4-5, 8-9) and are listed in Table I. Arc-shaped fracture-mechanics specimens having the shape and dimensions shown in Figure 1 were fabricated from the forgings and weldments.

Weldments were produced from forgings of either Type 304L or Type 21-6-9 steel and by cutting grooves along the length of the forging and filling each groove using the Gas Tungsten Arc (GTA) process and Type 308L stainless steel filler wire. The weld wire was war reserve quality and purchased from the National Security Campus in Kansas City. After welding, the forgings were sectioned into round discs and radiographed to verify that there was no unusual porosity, cracks, or other macroscopic defects from the welding process. This was done to ensure that fracture toughness samples were machined from high-quality welds

and that any differences in properties could be solely attributed to the differences in ferrite content or microstructure and not weld defects. Material microstructures were characterized using standard metallographic techniques and transmission electron microscopy. The results of the transmission electron microscopy (TEM) characterizations have been reported previously (5-6).

Table I. Compositions of Stainless Steel Forgings, Plates and Weld Filler Wires (Weight %)

Material	Forging	Sample ID	Cr	Ni	Mn	P	Si	Co	Mo	C	S	N	O	Al	Cu
HERF*															
21-6-9	A4582	F97-X	19.4	6.4	8.5	0.021	0.33			0.04	<.001	0.28	0.0022	<.001	
CF**															
21-6-9	B7073	H94-X	19.1	6.7	9.9	0.01	0.41			0.03	0.004	0.28	0.001	0.005	
CF**															
21-6-9	B6275	F9-X	19.3	6.7	9.9	0.01	0.38			0.03	0.001	0.28	0.002	0.004	
Filler Wire															
308L	308L Weldment	98-X	20.5	10.3	1.56	0.006	0.5	0.068	<0.01	0.028	0.012	0.055	-	-	0.015

*High-Energy-Rate Forged
**Conventionally Forged
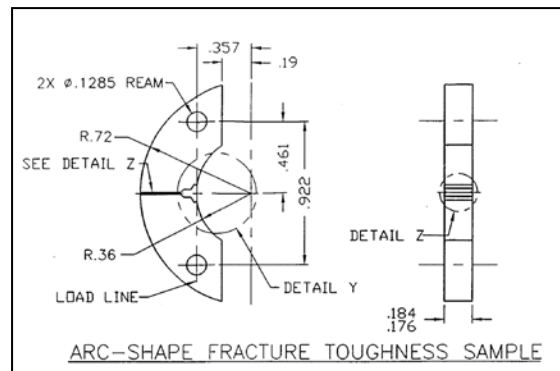
Figure 1. Shape and Dimensions in Inches of Fracture Toughness Sample.

Tritium exposures were conducted at 623 K and an over-pressure of 5000 psia. Decay helium concentration was measured in multiple steel specimens for two different aging times, 18 and 60 months, at Pacific Northwest National Laboratory. The specimens were analyzed for decay-helium content by isotope-dilution gas mass spectrometry following vaporization in a resistance-heated graphite crucible in a vacuum furnace. The helium concentration for the specimens of this and the earlier studies are listed in Tables X and XI and ranged from about 80 to 600 appm, depending on the steel type, weld ferrite content, and aging time. Included in the table are weldments of higher ferrite contents described in earlier reports ( ). For these new results, the longest-age base metals are estimated to have more than 1400 appm helium. This is based on the additional decay time and earlier measured values of decay helium from samples in the earlier test matrix (10-11). The long-aged weldments have lower hydrogen solubility and faster off-gassing, were estimated to have just ~600 appm helium.

It is noted that all measured decay helium levels were lower than expected. Figure 2 shows estimated tritium concentration values for Types 304L and 21-6-9 stainless steels based on standard solubility values. Also shown in Figure 2 are the tritium content of the specimens calculated from the measured decay helium values. Similarly, Figure 3 shows estimated decay helium levels and measured and calculated values during the 17 years of aging. In reviewing the decay helium measurement technique, it was discovered that the entire 1 mm thick slab of material for each specimen that was sent for analysis was not used. Instead, small pieces were cut from the near-surface corners. These corner areas would have lower decay helium levels because they are subject to the largest amount of tritium off-gassing during the furnace cooldown from the charging temperature. Also, they would be subject to off-gassing losses during aging. Further measurements will be needed to confirm this measurement error. Until proven otherwise, the data in this study will estimate the decay helium levels from the measured values, although the specimens could actually contain much more helium than these. It should also be noted, that the crack tips would also be subject to depleted helium because of tritium off-gassing losses. Since the fracture toughness measurements result from the point the crack first propagates, the crack could very well be in a depleted helium region. This could mean that the measured helium levels are consistent with the values in the crack tip region.

J-integral tests were conducted at room temperature in air using a screw-driven testing machine and a crosshead speed of 0.005 in / min. while recording load, load-line displacement with a gage clipped to the crack mouth, and crack length. Crack length was monitored using an alternating DC potential drop system and guidelines described in ASTM E647-95. The J-Integral versus crack length increase (J vs. da) curves were constructed from the data using ASTM E1820-99 (21). The J_Q value is defined as the material fracture toughness and was obtained from the intercept of an offset from the crack tip blunting line with the J-da curve. The blunting line was constructed with tensile properties of non-charged companion materials previously tested (1).

Table II Helium Concentration Tritium-Exposed Specimens (Aged 1.8 years)

Steel Type and Sample No.	Mass[a] (mg)	Measured ^{3}He (10^{15} atoms)	Helium Concentration (appm)[b] Measured	Average[c]
304-1	0.968	0.8943	84.76	85.6
	2.018	1.900	86.38	±1.1
304-2	3.528	2.620	68.13	68.1
	2.559	1.900	68.12	±<0.1
316LN-1	4.300	4.218	89.99	91.3
	5.261	5.310	92.60	±1.8
316LN-2	3.192	2.293	65.90	65.7
	2.365	1.687	65.44	±0.3
D49-4	3.313	1.602	44.36	51.9
	3.893	2.522	59.43	±10.7
98-12	1.736	2.287	120.9	123
	3.773	5.147	125.2	±3
412-8	1.486	1.053	65.01	71.3
	2.934	2.483	77.64	±8.9
912-10	3.758	4.475	109.2	111
	4.065	4.981	112.4	±2
8309-4	1.130	0.9872	80.15	88.7
	4.296	4.554	97.25	±12.1
8312-2	2.832	2.429	78.69	84.3
	3.227	3.162	89.90	±7.9
F4-37	2.333	3.400	133.7	129
	4.293	5.774	123.4	±7
F9-27	1.805	3.953	200.9	161
	5.389	7.115	121.1	±56
F97-27	2.375	5.321	205.5	212
	3.563	8.509	219.1	±10
EBA-2	3.168	2.690	77.90	86.0
	5.784	5.933	94.11	±11.5

[a]Mass of specimen for analysis. Mass uncertainty is ±0.002 mg.
[b]Helium concentration in atomic parts per million (10^{-6} atom fraction) with
 respect to the total number of atoms in the specimen. Uncertainty is estimated to
 be ±1%.
[c]Mean and standard deviation (1σ) of duplicate analyses.

Table III   Helium Concentration Tritium-Exposed Specimens (Aged 4.8 years)

Sample No.	Mass[a] (mg)	Measured ^{3}He (10^{15} atoms)	Helium Concentration (appm)[b] Measured	Average[c]
F4-17	3.86	12.56	298.5	291
	2.88	8.924	284.4	±10
F9-35	6.01	39.57	604.0	592
	4.49	28.35	579.3	±17
F97-14	5.17	33.75	598.9	612
	2.48	16.91	625.6	±19
H94-61	4.02	21.86	498.0	483
	2.62	13.36	467.8	±21
48A-6	2.72	6.281	211.9	216
	2.30	5.520	220.2	±6
49-7	1.44	1.316	83.8	81
	1.82	1.551	78.3	±4
412-7	2.17	2.828	119.6	114
	1.23	1.448	108.0	±8
98-9	5.26	20.78	362.4	371
	3.71	15.32	378.8	±12
912-12	2.06	2.985	132.9	112
	2.30	2.260	90.2	±30
8309-3	1.71	2.611	140.1	203
	4.27	11.15	239.6	±55
	2.95	7.412	230.5	
8312-3	3.86	9.874	234.7	254
	2.86	8.546	274.1	±28
EBA-4	3.09	7.377	219.0	298
	3.76	12.84	313.3	±73
	6.79	26.84	362.6	

[a]Mass of specimen for analysis. Mass uncertainty is ±0.02 mg.
[b]Helium concentration in atomic parts per million (10^{-6} atom fraction) with respect to
  the total number of atoms in the specimen. Uncertainty is estimated to be ±1%.
[c]Mean and standard deviation (1σ) of replicate analyses.
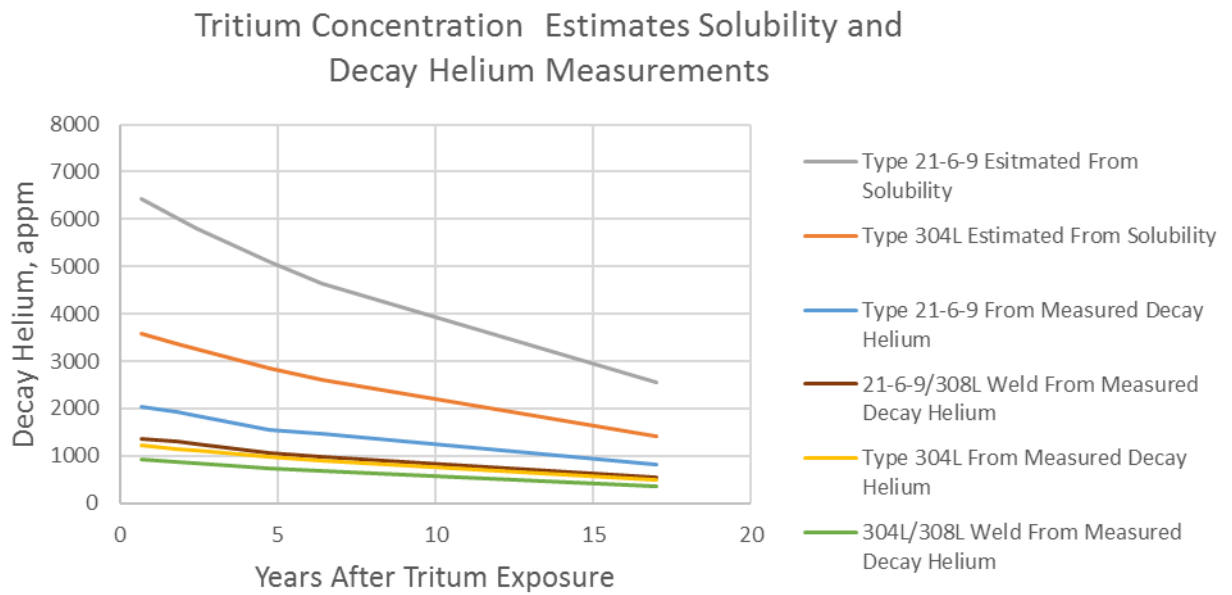
Figure 2 Tritium concentration estimates from solubility values and decay helium measurements
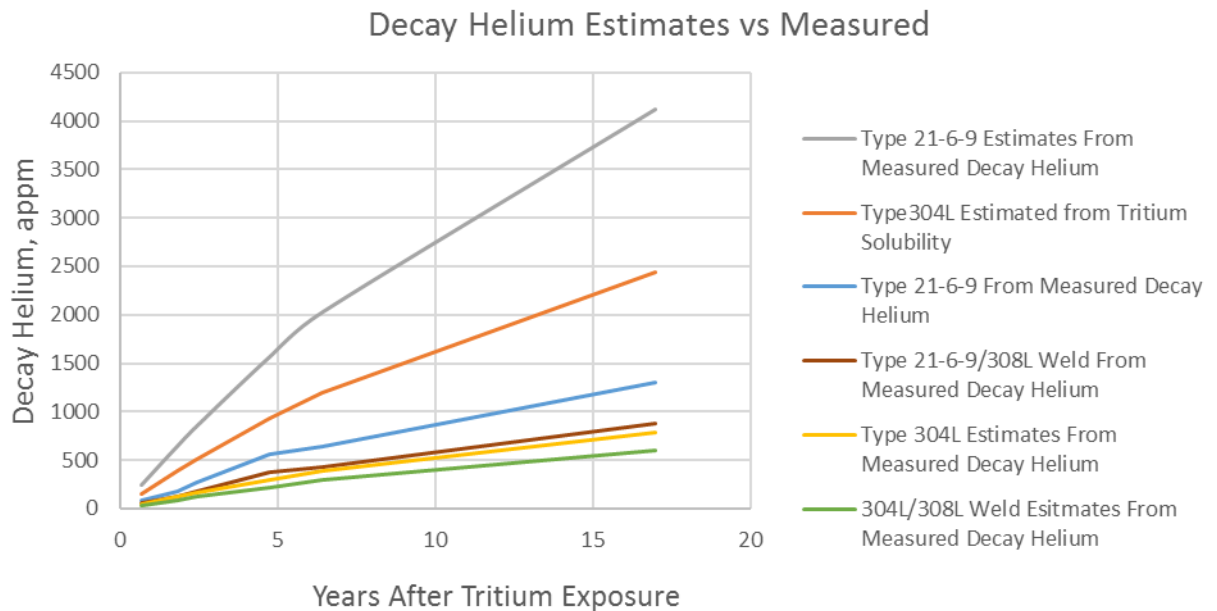
Figure 3 Decay Helium concentration estimates from tritium solubility values and decay helium measurements

III. RESULTS

A. TRITIUM EFFECT ON FRACTURE TOUGHNESS PROPERTIES OF LONG-AGED STAINLESS STEELS AND ITS WELDMENTS

Typical load-displacement records observed over the course of the study during the fracture toughness tests for base metals and weldments are shown in Figure 4. Note the large changes in the shapes of the load-displacement records caused by decay helium. The area under the load-displacement diagram during the fracture toughness test represents the energy of fracture and is a rough indicator of the toughness of the alloy. From the area specific geometry factors for the C-specimen, and the crack length measurements collected during the test, the actual fracture toughness value, J_Q is calculated by using the standard ASTM procedures, in this case - ASTM E1820-99 (16). The new results are listed along with selected values from the earlier data sets in Table IV. Generally, fracture toughness values were calculated from an average of two base metal tests and three weld metal tests.
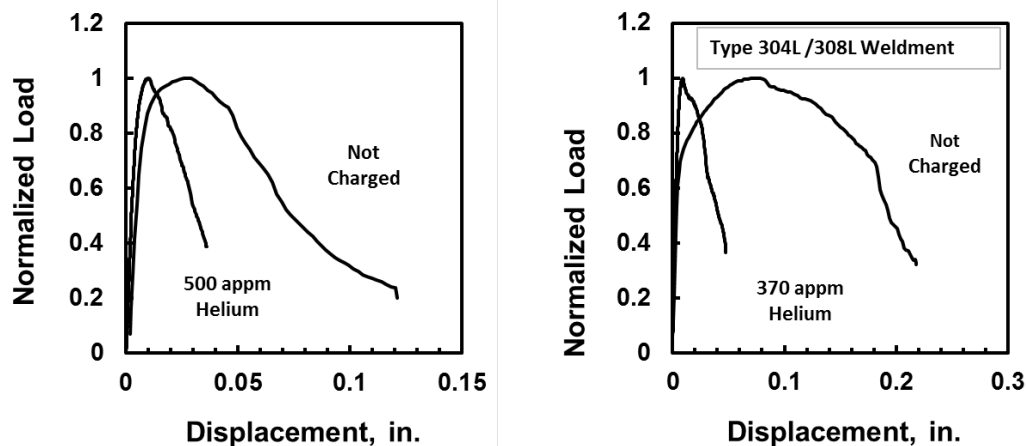
Figure 4. Typical Load-Displacement Records for Non-charged and Tritium-Charged Type 304L Base Metals and Welds. (Normalized Load Used in Plots Because Samples Have Different Initial Crack Lengths)

Table IV MECHANICAL PROPERTIES, FRACTURE TOUGHNESS VALUES, AND DECAY HELIUM CONTENTS OF BASE METALS AND WELDMENTS

Material Description		Mechanical Properties		Fracture Toughness Values				
	Ferrite	Yield Strength	Ultimate Strength	J_Q As-Received	J_Q Tritium-Charged & Aged 6 Mos.	J_Q Tritium-Charged & Aged 30 Mos.	J_Q Tritium-Charged & Aged 68 Mos.	J_Q Tritium-Charged & Aged 195 Mos.
Specimen ID	Ferrite%	ksi	ksi	lbs / in.	lbs / in.	lbs / in.	lbs / in.	lbs / in.
H94 Forged Type 21-6-9	~0	99.4	139.3	2114	1399	548	139	41
F97 HERF Type 21-6-9	~0	104.8	139.4	1203	689	402	163	38
F4-Forged Type 304L	~0	67	105	1690	1024	1117	901	
48-Normal Ferrite Weldment Type 304L/308L	8	62	88	4975	1890	1494	945	753
98-21-6-9/308L	6	60.3	98.8	3246	1605	300	420	
49-High Ferrite Weldment Type 304L/309L	33	83.0	108	711		275		161

The effect of tritium exposure and aging on the long-aged Type 304Land Type 21-6-9 base metal and their weldments are shown in Figures 4 through 8. The observation continues that tritium exposure lowers the fracture toughness properties of both base metals and weldments. This was characterized by lower J_Q values and lower J-da curves with increasing decay helium content. New results in Table IV show that the fracture toughness properties of Type 21-6-9 forged stainless steel were reduced by tritium and decay helium to about 2-4% of its as-forged value for the highest decay helium contents. Weldment fracture toughness properties were reduced to about 15% of the uncharged value for decay helium levels up to ~600 appm.
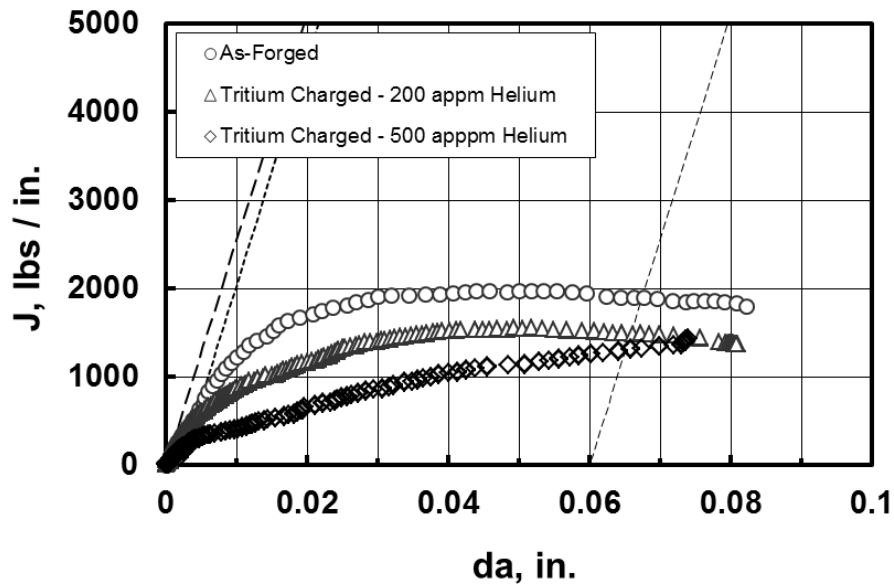
Figure 5. J-Integral vs. Change-in-Crack Length, J-da, Behavior for Non-charged and Tritium-Charged-and-Aged Type 304L Stainless Steel Base Metals.
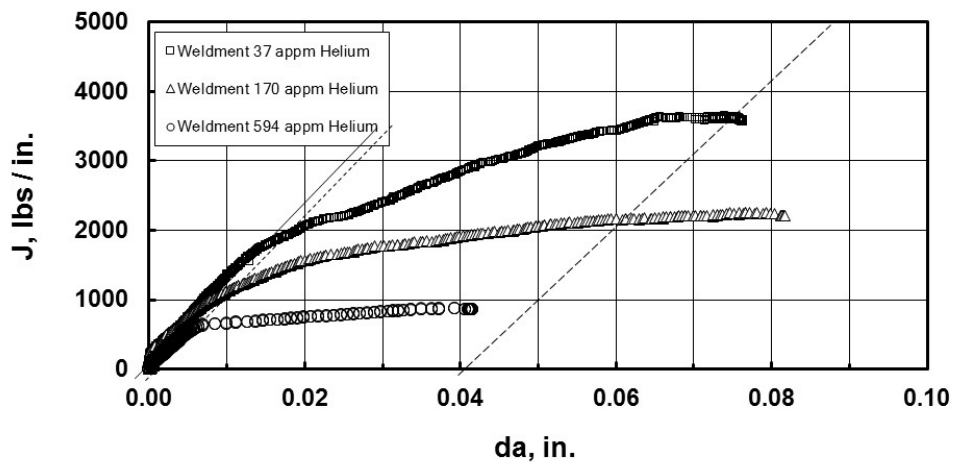
Figure 6. J-Integral vs. Change-in-Crack Length, J-da, Behavior for Non-Charged and Tritium-Charged-and-Aged Weld Metals. New Data is Shown in the Lower Curve for 594 appm Decay Helium.
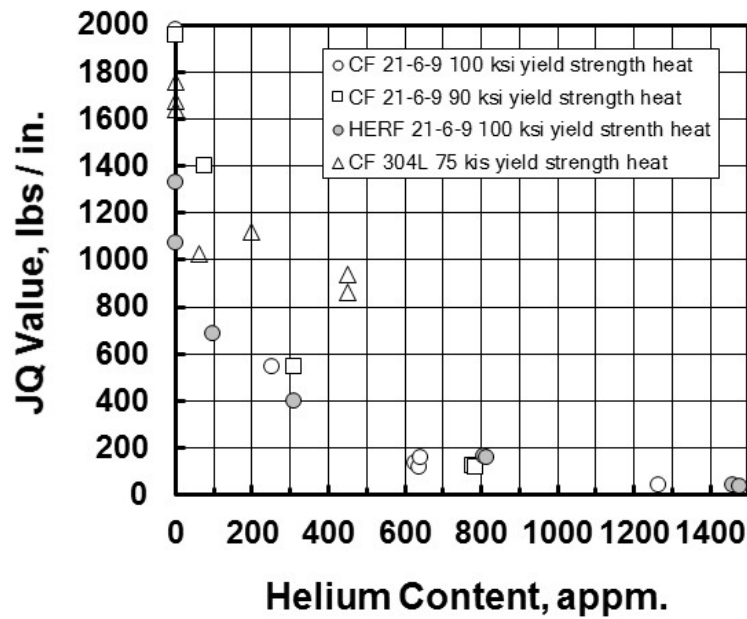
Figure 7. Fracture Toughness Reduction with Increasing Helium Content For Types 304L and 21-6-9 Stainless Steel Base Metals. Included are Data from Earlier Studies (1-2). New Data Shown are for Decay Helium Content Greater than 1000 appm.
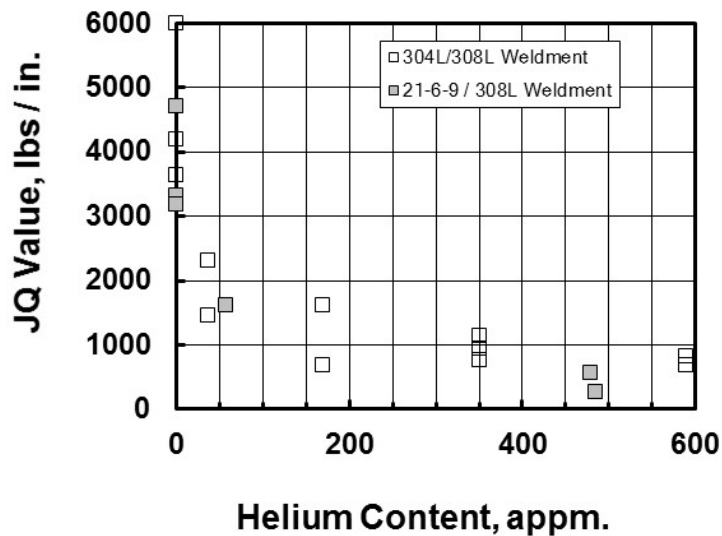
Figure 8. Reduction in Fracture Toughness with Increasing Helium Content of Types 304L and 21-6-9 Weldments. Included are Data from Earlier Studies. New Data are High-Helium Types 304L and 21-6-9 Weldments.
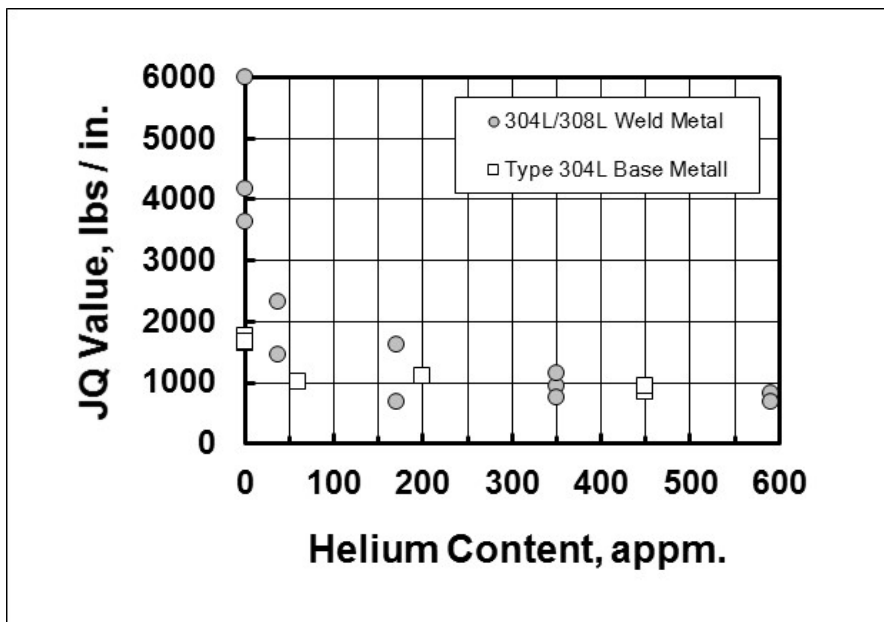
Figure 9. Comparison of the Reduction in Fracture Toughness with Increasing Helium Content of Types 304L Base Metal and Weldments. Included are High Helium Data from Earlier Studies.

B. TRITIUM PRECHARGING OF TYPES 304L AND 21-6-9 STAINLESS STEELS AND HEAT-AFFECTED ZONES

Tritium precharging was conducted on Types 304L and 21-6-9 stainless steel fracture mechanics bend bars supplied by Sandia National Laboratory. Table V shows the material compositions for the base metals and filler metals that are being used for the weld heat-affected zone study. Briefly, three-point bend bars were machined from the weld rings shown in Figure 10. Specimens were fatigue pre-cracked, Nitradd cleaned, and loaded into the tritium charging vessel just prior to the tritium charging run completed in October 2017. The specimen identifications are listed in Table V.

The gas composition is shown in Table VI along with the details of the time-temperature-pressure history. The charge run was started in late July, 2017, but unfortunately, it could not be completed continuously. A thermocouple failure after five days caused an interruption and a shutdown. Repairs were made and verification tests run. Charging could not be resumed immediately because of the delays from the repairs and other scheduled operations in the loading line. The vessel was refilled in Late September, 2017 and the charging run resumed. Later, another day-long outage occurred because of diesel backup tests in the entire Tritium facility. The run was completed on October 9 before the heater was cut off. Figure 11 depicts the time-temperature-pressure history listed in Table VII. Initial fracture toughness tests will be conducted during 2Q18 and later tests at higher decay helium contents during FY20 and beyond.

Table V Chemical Compositions (wt%) of Base Metal and Filler Metal SNL Welds and HAZ Specimens

Material	Fe	Cr	Ni	Mn	Si	C	N	P	S
304L	Bal.	19.38	10.44	1.72	0.57	0.027	0.02	0.021	0.002
21-6-9	Bal.	21.06	7.16	9.11	0.53	0.031	0.28	0.015	0.001
308L Filler	Bal.	20.5	10.3	1.56	0.50	0.028	0.055	0.006	0.012

(a)   (b)

Figure 10. Stainless Steel Welded Rings: (a) 21-6-9 with 308L Filler Metal and (b) 304L with 308L Filler Metal.

TABLE VI – Tritium-Charged TYPE 304L and 21-6-9 Stainless Steel Weldment and HAZ Bend Bars

Tritium Charge Vessel: SN 02151151-4 Source	Material	Sample ID	Sample ID	Sample ID
SNL HAZ & Weldments				
Type 304L Fusion Weld	304L	4FW-1	4FW-2	4FW-3
Type 304L Fusion Weld	304L	4FW-4	4FW-5	4FW-6
Type 21-6-9 Fusion Weld	21-6-9	9FW-1	9FW-2	9FW-3
Type 21-6-9 Fusion Weld	21-6-9	9FW-3	9FW-4	9FW-5
Type 304L HAZ	304L	HAZ A6	HAZ-A8	ZAZ-A9
Type 304L HAZ	304L	HAZ A10	HAZ A11	HAZ A12
Type 21-6- HAZ	21-6-9	HAZ B1	HAZ B2	HAZ B3
Type 21-6- HAZ	304L	HAZ B4	HAZ B5	HAZ B6
Type 304L Fusion Weld	304L	4FW-7	4FW-8	4FW-9
Type 304L Fusion Weld	304L	4FW-10	4FW-11	4FW-12
Type 21-6-9 Fusion Weld	21-6-9	9FW-7	9FW-8	9FW-9
Type 21-6-9 Fusion Weld	21-6-9	9FW-10	9FW-11	9FW-12
Type 304L HAZ	304L	HAZ A13	HAZ A15	HAZ 16
Type 304L HAZ	304L	HAZ A17	HAZ A18	HAZ A18 & A14
Type 21-6- HAZ	21-6-9	HAZ B7	HAZ B8	HAZ B9
Type 21-6- HAZ	21-6-9	HAZ B10	HAB B11	HAZ B12

Start Date: Jun-17

End Date: Oct-17   Total Samples: 49

Peak Charging Pressure: 4896 psi   Peak Charging Temperature: 349 C
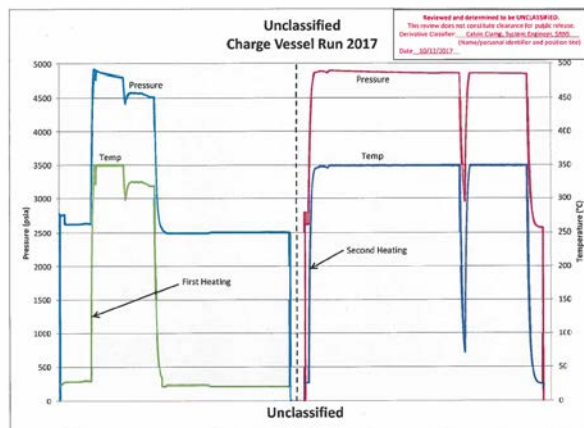
Figure 11– Weld and HAZ Specimen Tritium Precharging Time-Temperature-Pressure History

Table VII -Tritium Charging Run 2017 -Welds and HAZ for SNL

```
DATE              Temp°C  PSIA  Comment
7/23/2017 14:00    26     0
7/23/2017 15:00    26     2788  Fill
7/23/2017 16:55    26     2615
7/23/2017 20:30    27     2615  Heater On
7/24/2017 16:45    348    4891
7/28/2017 14:47    349    4790
7/28/2017 18:57    297    4410  TC Failure
7/29/2017 4:27     325    4574
7/30/2017 20:17    318    4515
7/31/2017 8:32     22     2564
8/9/2017 9:46      22     2502
8/9/2017 11:39     22     0     Unload
9/23/2017 14:00    26     0.1
9/23/2017 14:55    26     2789  Reload
9/23/2017 20:25    26     2615  Heater on
9/24/2017 16:37    349    4889
9/25/2017 3:52     346    4869
9/25/2017 8:25     349    4892
10/4/2017 13:23    349    4856
10/4/2017 21:44    72     2956  diesel backup test
10/5/2017 6:13     349    4846
10/9/2017 7:42     349    4842
10/9/2017 13:06    100    3170
10/9/2017 15:49    50     2780
10/10/2017 9:29    24     2560
10/10/2017 9:35    24     0
```

```
Fill       Mole %
T2         99.576
He3        0.366
D2         0.052
O2         0.001
Inerts     0.005
Total      100
```

C. SMALL ANGLE NEUTRON SCATTERING EXPERIMENTS

Small angel neutron scattering (SANS) is being used to probe tritium exposed steels. The purpose is to learn as much as possible about decay helium bubble size, spacing and distribution. The data are needed for developing deformation and cracking models for stainless steel. Transmission electron microscopy has been used to characterize helium bubble microstructures in tritium charged stainless steels (9) but the technique is unable to resolve bubbles that are smaller than 1 nm, nor can it easily resolve bubbles that are in heavily dislocated microstructures like forged steels. The TEM technique relies on strain contrast to image bubbles, and the strain contrast from dislocations masks the bubbles (9). TEM will continue to be used where it is most effective - for characterizing small areas/volumes in welds, heat-affected zones and annealed steels. SANS should complement the TEM observations and provide data for more complex microstructures, as well as a broader statistical representation of the materials in question.

Neutron scattering measurements were performed on tritium exposed stainless steel samples on beamline CG-2 at the High Flux Isotope Reactor (HFIR) at Oak Ridge National Lab (ORNL). The measurements were performed during one day of beamtime (12/2/17) granted through the general user proposal process. Two types of measurements were performed. Small angle neutron scattering (SANS) measurements were performed to elucidate the nature of Helium bubble formation in the matrix, and small angle incoherent neutron scattering (SAINS) measurements were performed to measure the hydrogen content in the samples.

The samples chosen for the study are detailed in the table below. The samples were chosen to study similar tritium exposed stainless steels aged for different times, as well as the effect of weldments on the formation of helium bubbles and hydrogen retention.

Sample	Charging	Age
304/308 filled steel weldments	T2	17-year
high energy rate forged 304	T2	3-year
304/308 filled steel weldments	H2 (5000psi)	N/A
304/308 filled steel weldments	H2 (10000psi)	N/A
304L/308 filled steel weldment	uncharged	N/A
High energy rate forged 304 steel	uncharged	N/A

Prior to performing the measurements, the samples were machined from previously studied fracture toughness specimens at SRNL using both hot (tritium-charged) and cold (not charged) EDM facilities. Shown in Figure 1a the geometry of the samples neutron scattering samples was chosen to maximize the cross section from the available fracture toughness specimens. The SANS samples (Figure 1b) were also cut to 0.5mm thick to minimize multiple scattering during the neutron measurements. Additionally, a sample cell was developed for the tritiated samples to allow them to be handled openly in the low rad areas of the neutron facility. The cell consisted of two zero length ConFlat viewports (1.33" dia.) for confinement and an Aluminum washer to hold the samples in place (Figure 1c/d). The viewport is made of high purity quartz to minimize scattering of the incident neutrons. The tabs on either side of the sample are designed to fit in a trough machined into the

aluminum washer to ensure the sample position does not vary during the measurements. Figure 1c shows the cell loaded with the Aluminum washer but no sample.

The tritium-precharged samples inside their cells were shipped in a DOT approved container. Prior to shipment calculations were performed to show that the activity was below the DOT limits, and all surfaces of every layer of the packaging were monitored for contamination prior to shipment. Importantly the sample cells ensured that no contamination could be transferred to the packaging. Finally, after arrival at Oak Ridge additional rad con surveys confirmed that no contamination was present anywhere on the package or on the outside of the sample cells.

Measurements were performed using a 2.5mm beam spot to allow for measurements in the HAZ and as-forged regions of welded samples. SANS and basic static SAINS measurements were performed on all the samples, and on both sides of the weld containing samples. On the protium containing welded samples, additional scanning SAINS measurements were performed scanning across the weldment in 0.1mm steps. Currently the raw data has been obtained but not reduced. Data reduction and analysis is nontrivial, but should be complete during Q2 of FY18.
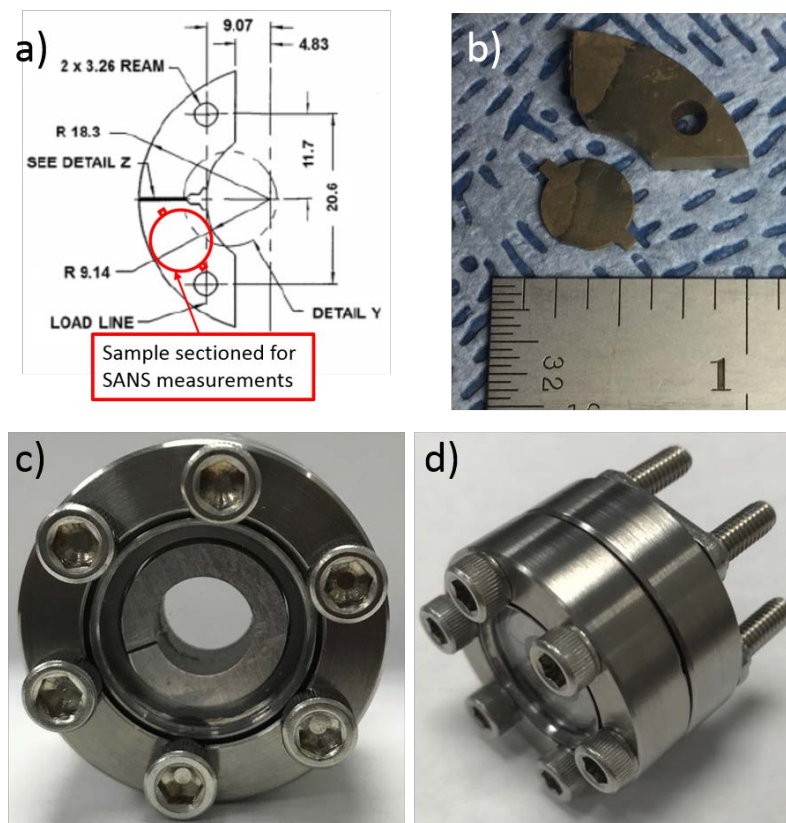

Figure 12: a) diagram of the geometry of the SANS samples machined from previously studied fracture toughness specimens at SRNL, b) picture of a SANS sample (note: the variation in color across the sample corresponds to regions of weld and base metal) c/d) samples cells designed for use in the neutron facility

D. TRANSMISSION ELECTRON MICROSOPY PROGRESS

Transmission Electron Microscopy is needed for characterizing the dislocation substructures in alloys and decay helium bubble microstructures after tritium exposures. The facility has not been used for several years and is being updated. For preparation of specimens from tritium exposed steels, a new jet polishing system was purchased from Struers. It is currently awaiting installation in SRNL. In the same lab, a radiological wash-down hood is available which is essential to this work for two reasons: 1) Polishing steel samples for TEM is done using dilute perchloric acid which needs a wash-down hood due to its ability to form highly explosive crystals, and 2) Work on tritiated metals must be performed in a radiological hood. The hood is currently tagged out due to a drainage issue; however, it should be inspected for operation during 2Q18. One way around these issues is to purchase a Focused Ion Beam (FIB) to prepare samples. A modern FIB would be on the order of $2 million after installation. Currently, PNNL has a FIB that has been qualified to work with tritiated metals and samples are being sent to check the viability of the technique.

A digital camera was also purchased to upgrade the SRNL hot TEM (a JEOL 2010). The camera was purchased from Gatan and SRNL procurement department is currently finalizing the paperwork to allow Gatan to perform the installation. In the meantime, work has been conducted with the JEOL tech to ensure the TEM is still functioning well. Service has been performed on the TEM three times, including to temporarily resolve a slight vacuum problem. A more permanent solution is being discussed with JEOL. Due to site requirements, the pump cannot be rebuilt on site, so a replacement pump is being procured to avoid the rebuild process.

Below is a picture of latex nanoparticles observed on the phosphor screen of the SRNL TEM to confirm its functioning. The image was taken using 1.5million times magnification which shows that beam can still be well aligned. It is helpful to note that the particles in the image are similar in size to the He bubbles in tritiated steels.

Additionally, electric-discharge machining (EDM) was used to extract TEM discs from previously tested fracture toughness specimens. Selected short and long-aged specimens from this study were used as the source material. While machining the samples for our SANS experiments sheets were also cut to be used for TEM samples, however, further effort is needed to cut 3mm discs for the TEM samples. Due to water currents in the EDM the 3mm TEM discs can be hard to locate after machining which leads to many hours of downtime spent searching for the cut samples. To avoid this problem, a fixture was designed to fit around the EDM head that would catch the samples. Several iterations of the fixture were 3-d printed at SRNL and have been tested on the cold EDM, but not yet moved to the CA.
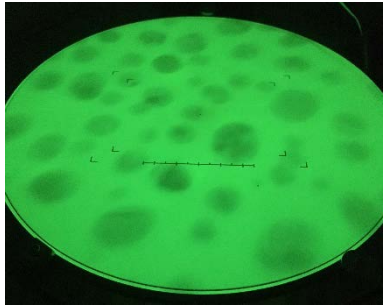
Figure 23: Image of latex nanoparticles on the phosphor screen of the SRNL TEM (the screen is at 1.5million x magnification).

Finally, specimens have been prepared for initial examinations after the facility is restarted. Interrupted tensile tests were conducted on two steels. The specimens were strained and unloaded at increasing levels of strain. The purpose is to characterize the deformation modes in the two stainless steels, Type 304L and 21-6-9 at different levels of strain and before and after exposure to hydrogen isotopes. For each steel, tensile specimens were unloaded after 1%, 5%, 10%, 25%, 35%, and 45% strain. TEM disks will be fabricated from the strained specimens and examined. Subsequent tests will be conducted on hydrogen-charged and tritium-charged-and-aged specimens in order to characterize the effects of hydrogen, tritium, and decay helium on the deformation modes. We are particularly interested in identifying the strain levels for the twinning modes of deformation because of the importance of twinning on the fracture process in aged steels.

E. Kelvin Probe Force Microscopy for Imaging Hydrogen in Stainless Steel Alloys

To gain a better understanding of the mechanism of hydrogen isotope interactions and embrittlement in stainless steel, Kelvin Probe Force Microscopy (KPFM) is being conducted. Atomic hydrogen in SS alloys segregates to regions of extended defects, such as grain and phase boundaries, and weakens the interfacial strength which can result in premature cracking: a process known as hydrogen embrittlement. The mechanisms of hydrogen embrittlement are depicted in Figure 14. Hydrogen segregated at the surface of stainless steel specimens and particularly at defect sites changes the local work function of the material, either by altering the local band structure and electronic state of the surface oxide or by inducing local strain fields.

Local variation in the surface work function can be measured by KPFM, which is conducted using an atomic force microscope (AFM). While traditional AFM imaging produces topography maps of surfaces with high spatial resolution (<1nm), KPFM produces surface potential (i.e., voltage) images by measuring the electrostatic forces between a metallized cantilever and conductive sample. By using a lock-in amplifier, the electric force between the AFM cantilever and the conductive sample can be nullified by

applying an external bias. The value of this applied voltage is used to calculate the local work function at each point in the topography image. Changes in the local work function of the material create contrast in KPFM image, and, depending on the polarity, will create images with dark or light features corresponding to changes in the local work function. Thus, the KPFM technique has the potential to co-locate the presence of hydrogen with extended defects at the surface, which should improve the capability of the long-term property prediction of an alloy in service. Directly imaging hydrogen segregation will improve our understanding of the effect of steel microstructure and processing on embrittlement.
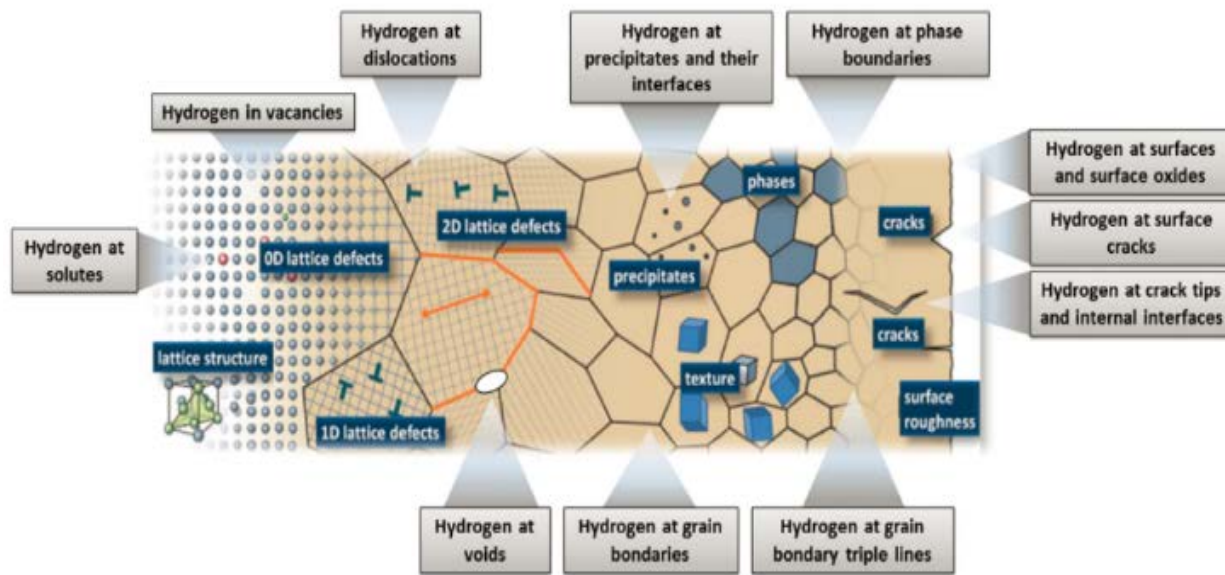

Figure 14. Hydrogen Embrittlement Phenomena and Microstructural Features Associated with Hydrogen Segregation.
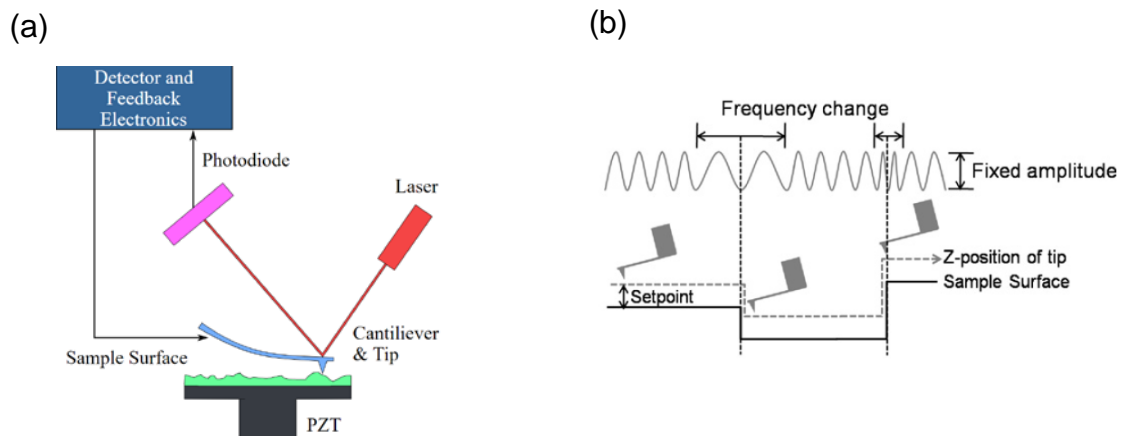

Figure 15. (a) Atomic force microscopy measures deflections between the cantilever and sample due to Van der Waals forces. (b) Modulations in the frequency of the oscillating

cantilever provide information on surface topography. Kelvin probe force microscopy measures the electrostatic forces between a metallized cantilever and conductive sample, which can be used to determine the local work function at the at the samples surface.

In this preliminary work, KPFM was used to examine austenitic SS specimens (type 304L) and weldments. The forged Type 304L stainless steel has large grains and less variation in elemental composition than the weldments. (Figure 21). So far, KPFM images indicate signatures of H segregation at twin boundaries (Figure 22), due to the significant variation in the local work function, seen as a dark contrast against the sample matrix. Furthermore, stainless steel welds show regions of skeletal ferrite and KPFM data suggest that these phases are possible locations for high hydrogen segregation (Figure 3).

So far, these preliminary studies show that KPFM can detect the presence of hydrogen. SEM and KPFM data show hydrogen associated with twin boundaries and weld ferrite. KPFM is an excellent complimentary technique for understanding the effect of hydrogen embrittlement. Future work will study the effect of thermal treatment and composition on the colocation of hydrogen in defects, and isotopic effects due to tritium.
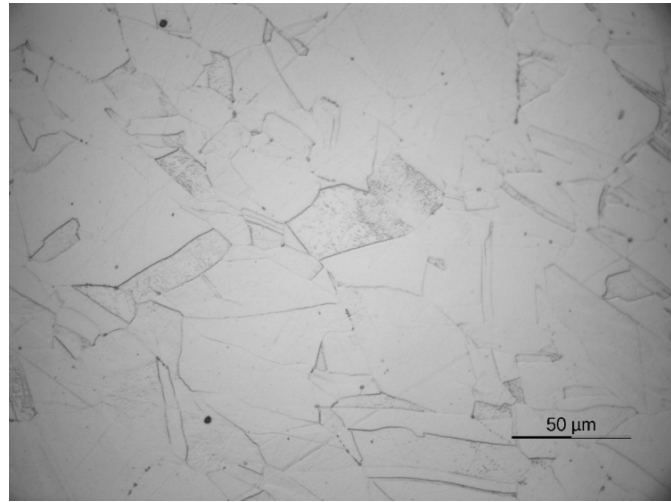
(a)
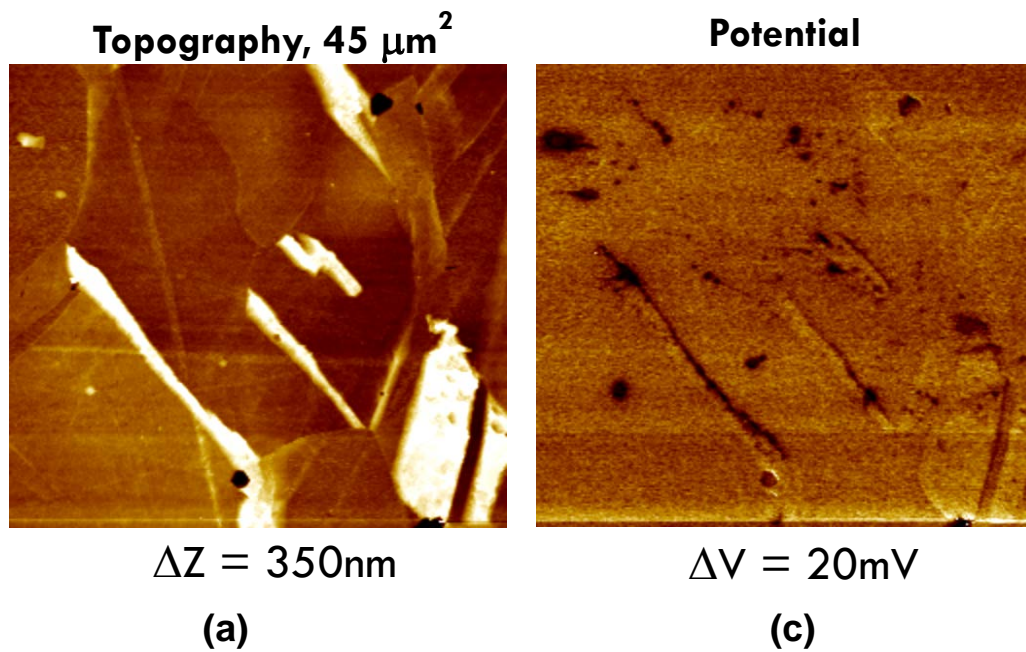
Figure 16 (a) Type 304L Stainless Steel Microstructure. (b) Topography Image Indicating Twin Boundaries and Steps. (c) KPFM Surface Potential images show high contrast (dark regions) which are indicative of enhanced hydrogen segregation at twin boundaries.
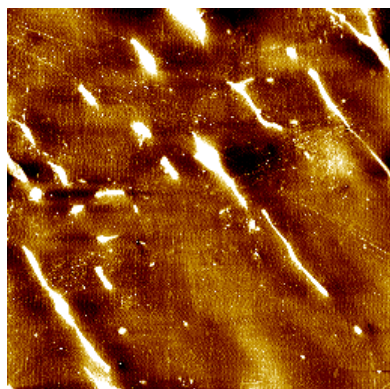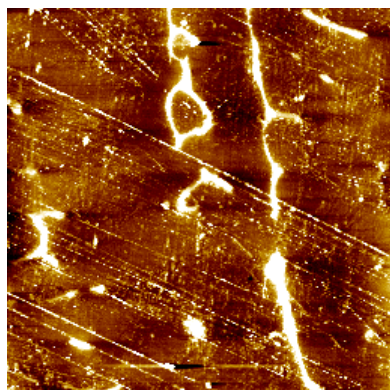
Topography, 45 μm^2   **Potential**
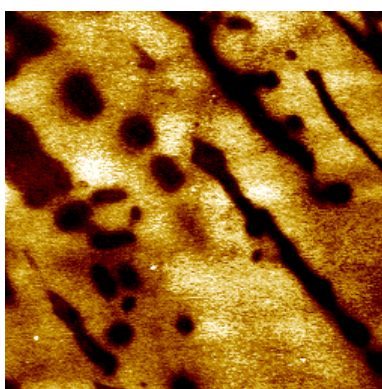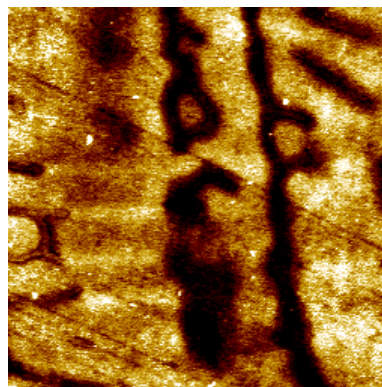
Figure 17 - Stainless steel welds (21-6-9/308L) show regions of skeletal ferrite in 308L region as possible locations for H segregation.

VII. SUMMARY CONCLUSIONS

The observation continues that tritium exposure lowers the fracture toughness properties of both base metals and weldments. This was characterized by lower J_Q values and lower J-da curves with increasing decay helium content.

- New results show that the fracture toughness properties of Type 21-6-9 forged stainless steel were reduced by tritium and decay helium to about 2% of its original value for a decay helium content of 1150 appm. Weldment fracture toughness properties were reduced to less than 20% of its original value for decay helium levels up to 500 appm.

- The Transmission-Electron Microscopy laboratory is being modernized after several years of inactivity. A new jet polishing system and digital camera were purchased and new techniques for fabricating TEM disks from tritium-exposed fracture specimens using EDM were developed and demonstrated. Specimens were extracted from the long-aged fracture specimens used in this study for future characterizations of the decay helium bubble microstructures.

- Neutron scattering measurements were performed on tritium exposed stainless steel samples, as well as hydrogen charged and uncharged controls on beamline CG-2 at the High Flux Isotope Reactor (HFIR) at Oak Ridge National Lab (ORNL) to elucidate the nature of decay helium bubble formation in stainless steels. The measurements were performed during one day of beamtime granted through the general user proposal process.

- Tritium pre-charging runs were conducted for SNL Weldment and HAZ specimens. Fracture toughness properties will commence during 2Q18 and will be the first ever conducted on tritium-precharged-and-aged HAZ specimens.

- KPFM was successfully used to detect the presence of hydrogen in forged and welded stainless steel. SEM and KPFM data show hydrogen associated with twin boundaries and weld ferrite. KPFM is an excellent complimentary technique for understanding the effect of hydrogen embrittlement.

VIII. FUTURE WORK

New decay helium measurements will be conducted at PNNL to further characterize the long-aged specimens. At the same time, the potential for using the contaminated focused ion beam instrument at PNNL for fabricating TEM disks from tritium-exposed specimens will be investigated, especially for fabricating specimens from the weld HAZs. Neutron scattering data will be analyzed for helium bubble size and spacing.

IX.   REFERENCES

1.   M.J. Morgan, "Hydrogen Effects on the Fracture Toughness Properties of Forged Stainless Steels", 2008 ASME Pressure Vessels and Piping Division Conference, July 27-31, 2008, Chicago, Illinois USA.

2.   M,J. Morgan, "Tritium Aging Effects on the Fracture Toughness Properties of Forged Stainless Steels", Proceedings of the Conference on Materials Innovations in an Emerging Hydrogen Economy, February 24-27, 2008, Cocoa Beach, Florida.

3.   M. J. Morgan, S. L. West, and G. K. Chapman, "Tritium Aging Effects on Fracture Toughness of Type 21-6-9 Stainless Steel", **WSRC-TR-2007-00244**, Savannah River National Laboratory, Washington Savannah River Company, Savannah River Site, Aiken, SC, June 14, 2007.

4.   Morgan, M.J.; West, S.; Tosten, M.H., Effect of tritium and decay helium on the fracture toughness properties of stainless steel weldment, Fusion Science and Technology Volume: 54 Issue: 2 Pages: 501-505: 2008.

5.   M. J. Morgan, M. H. Tosten, and S. L. West, "Tritium Effects on Weldment Fracture Toughness", **WSRC-TR-2006-00257**, Savannah River National Laboratory, Washington Savannah River Company, Savannah River Site, Aiken, SC, August 10, 2006.

6.   Michael J. Morgan and Glenn K. Chapman, "Forging Effects on Fracture Toughness Properties of Tritium-Charged-and-Aged Stainless Steels – Program Plan and Initial Results", **SRNL-TR-2011-00321**, November 2011.

7.   Michael J. Morgan, "2012 Accomplishments - Tritium Aging Studies on Stainless Steels", SRNL-TR-2013-00020, January 2013.

8.   M. H. Tosten and M. J. Morgan, "Microstructural Study of Fusion Welds in 304L and 21Cr-6Ni-9Mn Stainless Steels", **WSRC-TR-2004-00456**, Savannah River National Laboratory, Washington Savannah River Company, Savannah River Site, Aiken, SC, March, 2005.

9.   M. H. Tosten and M. J. Morgan, "Transmission Electron Microscopy Study of Helium-Bearing Fusion Welds", **WSRC-TR-2005-00477**, Savannah River National Laboratory, Washington Savannah River Company, Savannah River Site, Aiken, SC, November, 2005.

10.   M. J. Morgan and G. K. Chapman, "Cracking Thresholds and Fracture Toughness Properties of Tritium-Charged-and-Aged Stainless Steels", **WSRC-TR-2010-00393**, Savannah River National Laboratory, Washington Savannah River Company, Savannah River Site, Aiken, SC, December, 2010.

11.   S. L. Robinson, "The Effects of Tritium on The Flow and Fracture of Austenitic Stainless Steels", *Proc. Fourth Int. Conf. on Hydrogen Effects on Material Behavior*, A. W. Thompson and N. R. Moody, eds., The Minerals, Metals & Materials Society, Warrendale, PA, 1989, p. 433.

12.   S. L. Robinson and G. J. Thomas, "Accelerated Fracture due to Tritium and Helium in 21-6-9 Stainless Steel", *Metallurgical Transactions A*, 22A (1991), 879-885.

13.   ASTM E1820-99 "Standard Test Method for Measurement of Fracture Toughness", *1999 Annual Book of ASTM Standard Volume 3.01 Metals-Mechanical Testing; Elevated and Low-Temperature Tests; Metallography*, American Society for Testing and Materials, 1999.

14.   C. San Marchi, B.P. Somerday, "Permeability, solubility and diffusivity of hydrogen isotopes in stainless steels at high gas pressures", Intern J Hydrogen Energy 32 (2007) 100-116.

15.   G. R. Caskey, Jr., "Hydrogen Effects in Stainless Steels", *Hydrogen Degradation of Ferrous Alloys*, ed. J. P. Hirth, R. W. Oriani, and M. Smialowski, eds., (Park Ridge, NJ: Noyes Publication, 1985), p. 822.

16.   ASTM E1820-99 "Standard Test Method for Measurement of Fracture Toughness", *1999 Annual Book of ASTM Standard Volume 3.01 Metals-Mechanical Testing; Elevated and Low-Temperature Tests; Metallography*, American Society for Testing and Materials, 1999.